Geology, Geophysics & Environment 2022, vol. 48 (2): 89–110

Crustal deformation of the Central Indian Ocean, south of Sri Lanka as inferred from gravity and magnetic data

Sistla Ravi Kumar

Vignan's Institute of Information Technology, Duvvada, Visakhapatnam, India, e-mail: ravikumar25450@gmail.com, ORCID ID: 0000-0003-2440-9399

Received: 9 May 2021; accepted: 24 May 2022; first published online: 2 June 2022

Abstract: Bathymetry, gravity, and magnetic data across the Central Indian Ocean Basin (CIOB) along a WE track between 5°N to 1°N latitudes and 77°E to 90°E longitudes are used to identify crustal deformation due to tectonic features such as the Comorin Ridge, 85°E ridge, Ninety East Ridge, and major fracture zones. The tectonic features were interpreted along the North Central Indian Ocean using 2D gravity modelling to understand the origin and tectonic activity of the subsurface features. The Comorin Ridge is coupled with gravity anomalies with small amplitude varying 25–30 mGal in comparison with the ridge relief which suggests that the ridge is compensated at deeper depths. The focus of the present study is to prepare a reasonable crustal model of the Central Indian Ocean using gravity and magnetic data. The crustal depths of the Central Indian Ocean Basin (CIOB) determined from gravity data using the spectral method are compared with the 2D gravity modelling results. It has been observed that the crustal depths obtained from the Spectral method are in good correlation with results obtained from 2D gravity modelling. The average basement depths for the profiles were obtained as ~5 km and perhaps deviated approximately 1–2 km from the mean. In the case of curie isotherm, the crustal depths vary 9–12 km for all magnetic profiles which may indicate deformation.

Keywords: CIOB, deformation, tentative, basement, tectonic, 2D gravity model

INTRODUCTION

It is known that Sri Lanka, South India, and nearby oceanic areas occupy a region of negative gravity anomaly, as revealed by satellite observations and gravity measurements. Sri Lanka and the south of the Indian peninsula have steep continental shelves surrounded by the Indian Ocean on the eastern side of the Indian peninsula and have large extensive sediment accumulation known as the deep-sea Bengal fan. The extension of sediment accumulation towards the south is nearly 3000 km with a mean width of 1000 km. The greatest thickness of sediment is more than 20 km at the head of the Bay of Bengal (Curray & Moore 1971, Curray & Munasinghe 1991).

The bathymetry and free-air gravity maps of the Central Indian Ocean Basin (CIOB) are shown in Figures 1 and 2. The free-air gravity map (Fig. 2) of the Central Indian Ocean Basin (CIOB) explains the deformation as reflected in the gravity data (Haxby 1987) and has interesting implications for three prominent features of the north-eastern Indian Ocean, namely the Ninety East Ridge, the 85°E ridge, and the Comorin Ridge. Sclater & Fisher (1974) suggested that the change in ridge morphology may reflect the separation of Australia and Antarctica.

https://doi.org/10.7494/geol.2022.48.2.89 ISSN 2299-8004 | e-ISSN 2353-0790 | Wydawnictwa AGH

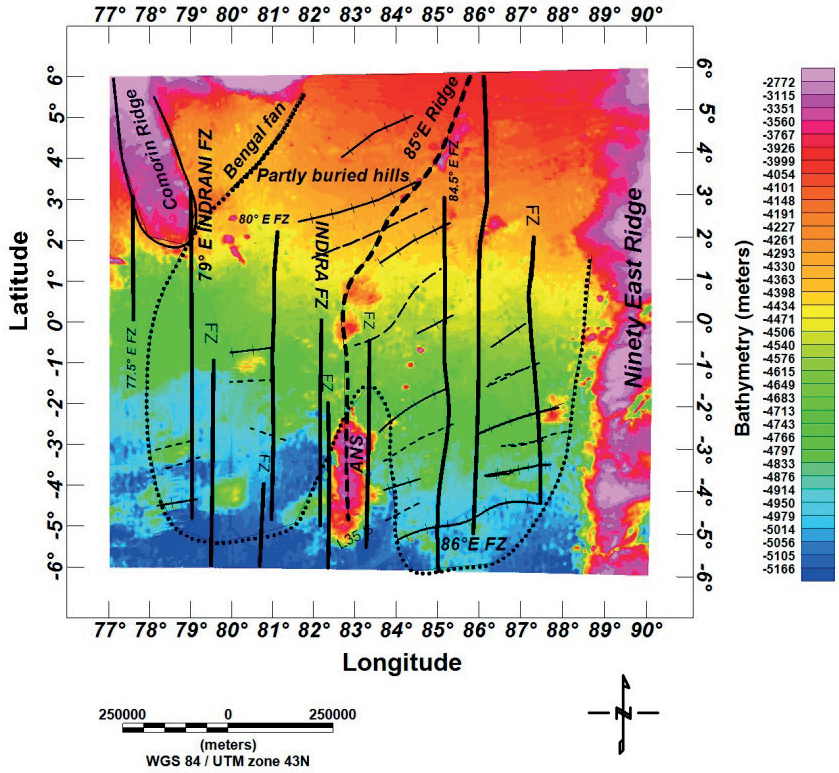

Fig. 1. *Bathymetry map of Central Indian Ocean, south of Sri Lanka showing basement undulations; crests (+++) and troughs (----) from Geller et al. (1983), major fracture zones (FZ) from Royer & Chang (1991) and Wessel et al. (2015), the limit of the Bengal Fan (.....)*

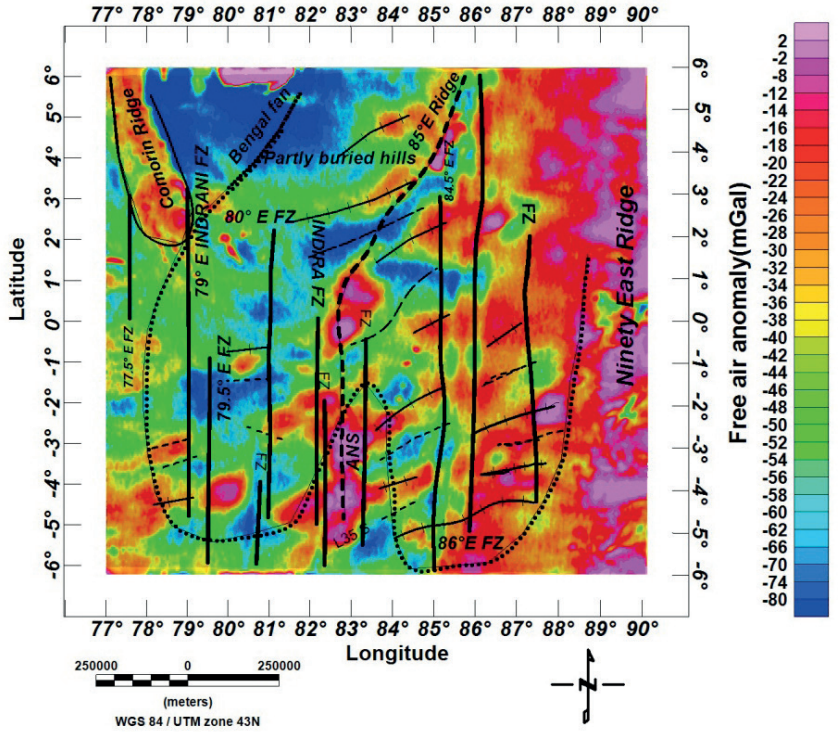

Fig. 2. *Free-air gravity map of Central Indian Ocean, south of Sri Lanka showing basement undulations; crests (+++) and troughs (----) from Geller et al. (1983), major fracture zones (FZ) from Royer & Chang (1991) and Wessel et al. (2015), the limit of the Bengal Fan (.....)*

The irregular morphology is associated with the region of highest seismicity (Stein & Okal 1978). Liu et al. (1982) identified the buried 85°E ridge that stretches from 18°N to 5°N and is characterized by a free-air gravity low which is identified from shipboard gravity and seismic reflection data. The shipboard gravity data for the region between ~1°N–5°N and ~85°E–87°E has a gap identified by them. So, the 85°E ridge may continue to the south as an undulation high at 3°N, south of Sri Lanka. The southern part of the 85°E ridge is interpreted earlier and reflects the recent deformation (Stein et al. 1989).

The tectonic deformation can be explained in two spatial scales based on the long-wavelength undulations (100–300 km) of the oceanic basement and shorter wavelength reverse faults (5–10 km) with connected folds. However, the earlier one penetrates throughout the deformed oceanic crust (Bull & Scrutton 1990). The folds connected with reverse faults take place in the hanging walls of reverse faults and are limited to the sedimentary layer (Bull & Scrutton 1990). Bull et al. (1992) found a relationship that the wavelength of folding is seven times the thickness of the brittle layer. The detailed analysis of the seismic reflection profiles (~5370 km) of the Central Indian Ocean Basin deformation zone (Krishna et al. 1998) confirmed the existence of long-wavelength (150–300 km) anticline basement structures with 1–2 km relief and tight folding and high angle faults (5–20 km long) along with the oceanic basement.

Krishna et al. (2002) observed a long-wavelength basement trough (nearly 150 km) which is deepened by one kilometre from the regional trend (northern dipping). This information was obtained from the analysis of the bathymetry, gravity, and seismic reflection data of the diffusive zone of the Central Indian Ocean Basin (CIOB). Horizontal crustal compressions in the diffusive plate boundary might be the reason for the formation of the basement trough as revealed by seismic analysis (Krishna et al. 2002). An attempt has been made to study the part of the crustal deformation of the Central Indian Ocean Basin (CIOB) lying between 5°N to 1°N and 77°E to 90°E through free-air and magnetic anomalies. As a preliminary analysis, the data has been interpreted by spectral and Werner deconvolution methods to arrive at a tentative crustal depth model which can be compared with the 2D gravity forward model.

During the rift phase of Madagascar, the Comorin Ridge originated about 90 Ma from the southwest of India and extends up to 500 km in the NNW-SSE direction. It is associated with low amplitude gravity anomalies which are ranging from 25–30 mGal compared to the ridge relief. This phenomenon suggests that the anomalies are compensated at deeper depths.

The southern region of the ridge lies between 1.5°N and 3°N has an elevation up to 0.5 km compared to the neighbouring ocean floor. The central part of the ridge lies between 3°N and 5°N has a maximum elevation of up to one kilometre compared to the surrounding ocean depths varying 3–4 km. In the north, the ridge has an elevation between 5°N and 6°N which is mainly towards the eastern side varying 0.4–0.7 km from neighbouring ocean depths of about 2.5 km. The western flank expands more than 100 km, having a relatively uniform gradient in the southern region of the ridge. The eastern flank precipitously deepens to around 1.2 km along a level surface of about 50 km. The analysis of Central Indian Ocean Basin (CIOB) data (Kahle et al. 1981) suggests that the Comorin Ridge is developed on the oceanic crust with an Airy type compensation mechanism. The eastern border of the Comorin Ridge indicates a margin between oceanic crust and rifted continental crust.

The 85°E ridge continues from the Mahanadi Basin to the Afanacy Nikitin Seamount (ANS) in the Central Indian Ocean. The ridge is coupled with a negative anomaly related to the north region which is up to 5°N latitude and the ridge is underlying the thick Bengal Fan sediments. The positive anomaly is above the south part, where the ridge is sporadically disclosed over the seafloor. The gravity anomalies of the ridge exist at three geological ages, named Late Cretaceous, Early Miocene, and the Present, for various crust-sediment structural configurations. The ridge was linked with an appreciable positive anomaly at the time of the Late Cretaceous with a compensation generated by a broad flexure of the Moho boundary. The variation of the initial gravity anomaly to the negligible positive anomaly of the ridge is due to enclosing post-collision sediments by the early Miocene. At present, the ridge is underlain by 3 km thick

Bengal Fan sediments on its crustal section, with pre- and post-collision sediments of 8 km thickness on its flanks. This environmental condition had transformed the slight positive gravity anomaly into a specific negative gravity anomaly.

The Ninety East Ridge is along the north of the equator in the Eastern Indian Ocean, is vigorously deforming and the ridge basement is elevated up to 2 km with the corresponding Bengal Fan. Seismic studies reveal the continuity of the ridge under sediments for 700 km north of 10°N, where the ridge plunges under the fan sediment. The ridge corresponds to a free-air gravity high of 50 mGal amplitude and 350 km wavelength, along with a strike continuity of 1500 km in a north-south direction. Regression analysis connecting gravity and bathymetry clearly states that the ridge's gravity field may not be explained exclusively by its altitude. The ridge gravity field becomes continuously restrained northwards, where overlying Bengal Fan sediments have a slighter density in contrast with the ridge material. The gravity analysis concludes that the ridge covers significant crustal mass anomalies consistent with the hot spot model. The anomalous mass is less dense by about 0.27 gm/cm^{-3} than the neighbouring oceanic upper mantle which acts as a "cushion" for the isostatic compensation mechanism of the ridge. The Ninety East Ridge (NER) north of the equator has a length of more than 1700 km, collectively with its buried continuation for 700 km below the Bengal Fan. The ridge is elevated by about 2 km concerning the neighbouring Bengal Fan oceanic crust, with an average width of about 350 km along the east-west direction. The ridge is regarded as a free-air high of 50 mGal and not the same over the entire extent of the Ninety East Ridge (NER). We can observe several gravity closures which suggest that the ridge consists of differential anomalous masses that vary on a local scale.

BATHYMETRY, SEDIMENT ISOPACH, FREE-AIR, AND MAGNETIC MAPS OF THE STUDY AREA

The magnetic and gravity profiles of the study area are along 77°E–90°E longitudes and 5°N–1°N latitudes are shown in Figure 3 is along with bathymetric data is extracted from ETOPO-1 (Amante & Eakins 2009) having one arc-minute (1′) global relief model of the earth surface.

The sediment isopach map (Straume et al. 2019) of the region (Fig. 4) indicates that the thickness of sediments reduces further to the south. The seafloor in this phase is especially smooth, with a north to south gradient and a discrepancy in sedimentary thickness corresponds to undulations in the basement topography (Curray et al. 1982).

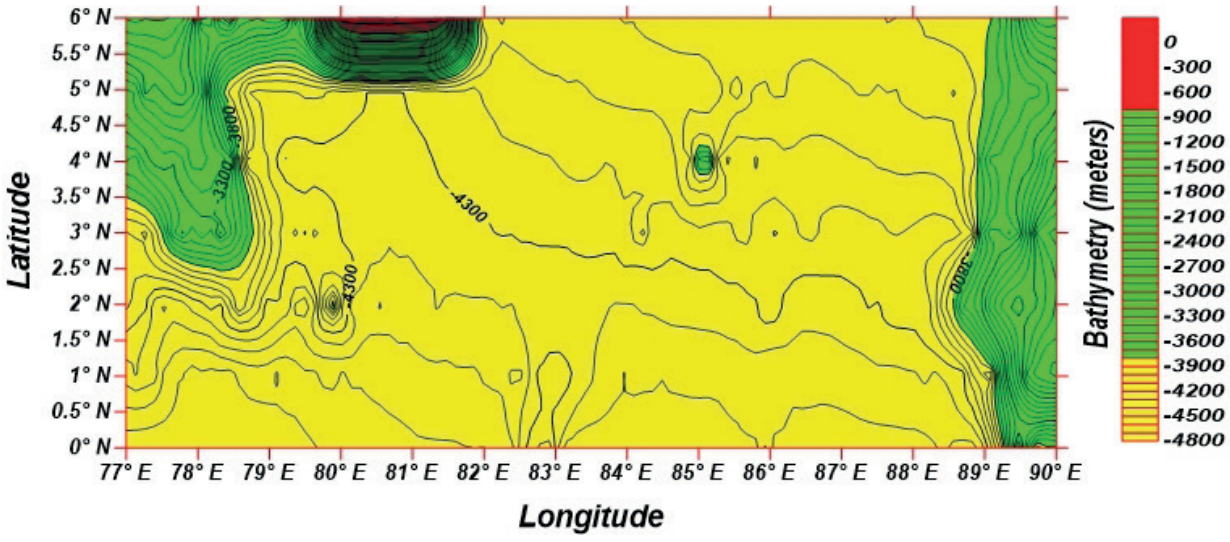

Fig. 3. *Bathymetry of Central Indian Ocean, south of Sri Lanka (Amante & Eakins 2009)*

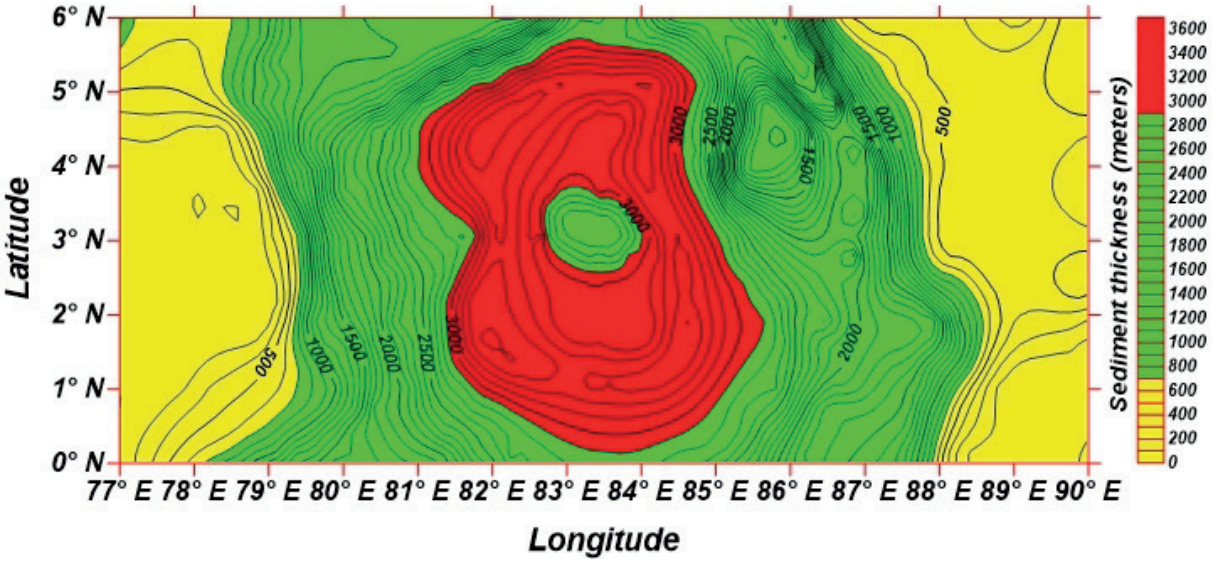

Fig. 4. *Sediments isopach map of Central Indian Ocean, south of Sri Lanka (Straume et al. 2019)*

The free-air gravity data (Fig. 5) is extracted from global one-minute grids (Sandwell et al. 2014) and digitized at the one-kilometre interval. The free-air anomaly data provides information below short wavelengths (<20 km) which is helpful in regional geophysical investigations.

The marine magnetic data (Fig. 6) is extracted from global two-minute grids (Maus et al. 2009) and digitized at the one-kilometre interval. It can be observed that the shape of the anomalies depends on thickness and susceptibility. Short wavelength magnetic anomalies of this region are indicative of shallow magnetic basement changes (Rabinowitz & LaBrecque 1977). It can be observed that the distinct anomaly closures (Figs. 5, 6) are either elongated in a NE-SW direction or circular from the free-air gravity and magnetic anomaly maps (Rao et al. 2004).

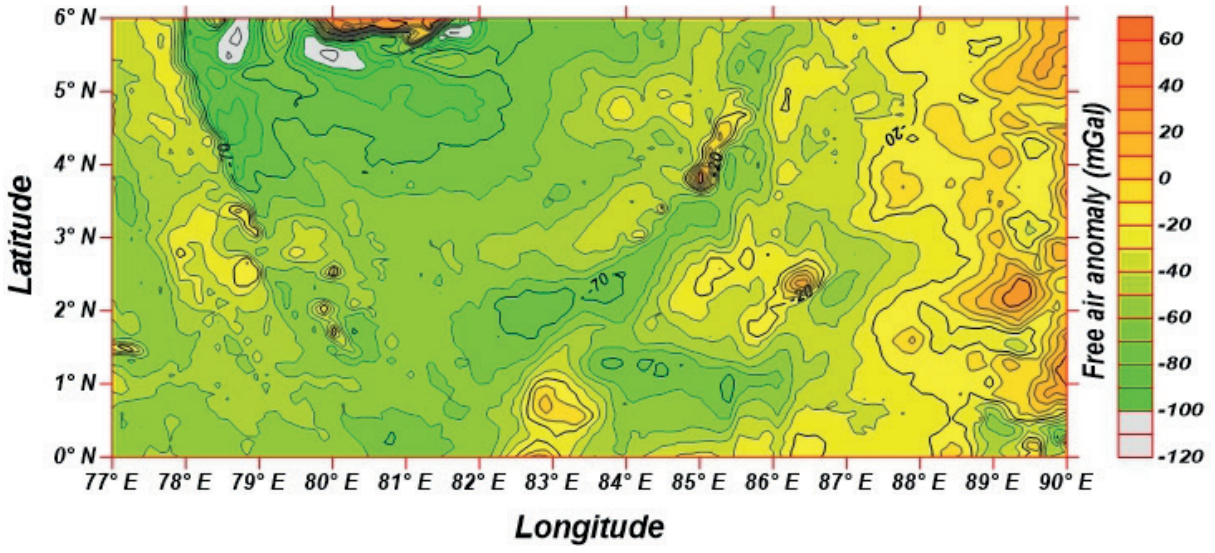

Fig. 5. *Free-air gravity map of Central Indian Ocean, south of Sri Lanka (Sandwell et al. 2014)*

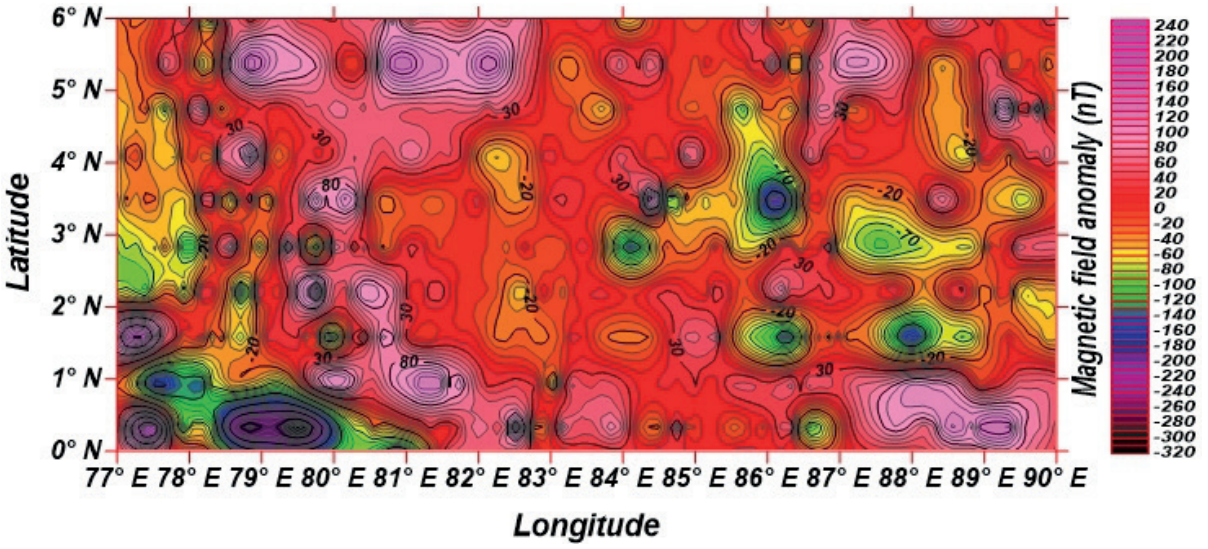

Fig. 6. *Magnetic field anomaly map of the study area, south of Sri Lanka (Maus et al. 2009)*

METHODOLOGY

Spectral and Werner deconvolution techniques are articularly useful to determine the depth of the causative sources which can be utilized in crustal modelling. Subrahmanyam & Gebissa (2017) carried out a performance analysis for these two techniques and showed the efficacy and limits of their usage for determining the tentative depths of causative geological features. Deformation of CIOB was observed along the north of the equator by interpreting the magnetic data with the spectral and Werner deconvolution techniques, and gravity data with the spectral method (Ravi Kumar & Subrahmanyam 2020).

The magnetic anomalies are interpreted with the spectral and Werner deconvolution methods and both of these methods give depth to the interfaces. Each magnetic profile is divided into several segments and the segmentation of anomalies was done with the knowledge of the magnetic lineation (age anomalies). Each segment overlaps with the adjacent segments by 5–10%. The magnetic anomalies are converted into the frequency domain and the amplitude spectrum is calculated. From this amplitude spectrum depths to the interfaces have been determined. To determine the deeper marker (Curie Isotherms), the anomalies have been filtered with a low pass filter to extract long-wavelength anomalies. Several frequencies (0.04 Hz, 0.06 Hz, 0.08 Hz, 0.10 Hz, and 0.12 Hz) were applied to extract the long-wavelength anomalies. The low pass filter of 0.08 Hz has been found suitable to represent the deeper interface of the oceanic crust. We can use unfiltered and filtered magnetic anomalies respectively of each segment to determine shallow and deeper depths with the Werner deconvolution method. The same procedure is carried out for all the profiles and tentative crustal depth models prepared.

The free-air anomalies are interpreted with the spectral method which gives depth to the interface. Each free-air anomaly profile is divided into several segments and each segment overlaps with the adjacent segment by 5–10%. The free-air anomalies are converted into the frequency domain and the amplitude spectrum is calculated. From this amplitude spectrum, depth to the interface has been determined. For determining the deeper marker, the anomalies have been filtered with a low pass filter to obtain the long-wavelength anomalies which may be due to deeper interfaces. A low pass filter of 0.08 Hz has been found suitable to represent the deeper interface of the oceanic crust. The same procedure was carried out for all the profiles and tentative crustal depth models prepared.

Spectral method

A spectrum expresses a function that is the dependence of some quantity on one or several independent variables. It represents the dependence of some function on one of several independent variables. The function may be amplitude, power or any other property, and the independent parameter is generally frequency or wave number. The spectrum is a statistical quantity with a definite mathematical expression, derived from time or space functions by certain transformations.

The simplest of the mathematical expressions can be expressed as a sine and cosine function representing a periodic data set of constant time intervals such as:

$F(t) = a \sin(\omega t)$

or:

$F(t) = a \cos(\omega t)$.

A continuous periodic function available over a specific interval $-T/2 < t < T/2$ is:

$$F(t) = \frac{1}{T} \int_{(-T/2)}^{(T/2)} F(\omega) e^{i\omega t}.$$

The power spectrum can be written as:

$A^2\omega = |F(\omega)| = [a^2(\omega) + b^2(\omega)]$.

The modified amplitude spectrum $A(\omega)$ plotted versus ω gives a straight line whose slope is equal to the average depth (Z) to the top of the source

$Z = (L/2\pi\ (f_2 - f_1))\ \ln\ (A_{f_2}/A_{f_1})$

where Z is the average depth to the source, L is the wavelength which is equal to the length of the profile being analysed, f is the spatial frequency, and A_f is amplitude.

Power spectral analysis measures the mean depth of the interfaces, taking into consideration the log of power of the Bouguer gravity spectrum as a function of wave number or frequency which assumes the uncorrelated distribution of sources (Spector & Grant 1970) or scaling nature of sources (Maus & Dimri 1994, 1995, 1996, Pilkington et al. 1994). The gravity anomaly spectrum due to the layered sources is split into multiple segments in the frequency domain which can be interpreted in terms of the mean depth to the interface. The high-frequency component needs to be filtered from the amplitude spectrum to obtain the low frequency, long wavelength anomalies which represent the depth to the deeper levels (curie isotherm).

Werner deconvolution method

Werner (1953) formulated the magnetic response of sheet-like bodies (thin dykes) with an infinite length and an infinite depth in terms of a linear equation where two of the unknowns are the location and the depth to the top of the thin dyke. This elaboration allows the effects of regional and interference between adjacent anomalies to be accounted for calculation of the depths and positions. They used this principle to produce an automatic routine that progressively samples magnetic field values along with profiles and determines the depths and positions of all the thin dykes on the profile.

The magnetic field of a body depends on its position and depth. It is possible to estimate the position of the top of the causative body and its magnetization from the total field. A profile of the observed total field over the causative body can be separated into groups of four or more and each group gives an estimate of the source position. When locations are plotted in cross-section then individual depth estimates tend to cluster around the true location of the sheet-like body. If the true geological section can be modelled by a collection of such bodies, then after analysing numerous groups of successive points along the profile may specify their location.

The Werner deconvolution technique is used for automated magnetic interpretations which are based on the thin-dike assumption (Werner 1953) and is useful for the linearization of complex nonlinear magnetic problems. The filtered and unfiltered magnetic anomaly segments used in calculating spectral depths for deeper and shallow markers have been subjected to the Werner deconvolution technique. The free-air gravity anomaly profile is divided into various segments and each segment anomaly data is transformed into the frequency domain. Spectral depths of each anomaly segment are estimated from the slope of the spectrum. Each anomaly segment is filtered with a low pass filter and the amplitude spectrum computed for each filtered anomaly segment and depths to the deeper features (Moho depth) determined.

RESULTS AND DISCUSSION

All the profiles are taken in the W-E direction between 77°E–90°E and the distance is about 1442 km. As mentioned in the methodology, each gravity and magnetic anomaly profile was divided into various segments and the amplitude spectrum is calculated for each anomaly segment.

The magnetic anomaly signal is filtered with a selected low pass filter (0.08 Hz) to obtain long wavelengths which represent deeper sources. The spectrum is calculated after the filtered signal is again transformed to obtain the best-fit slope of the low-frequency range of the spectrum. It gives depth to the deeper interface (or Curie isotherm) and the same procedure is carried out for all segments and basement depth is determined. These values are shown in Tables 1, 3, 5, 7, and 9. The Werner deconvolution technique is used for unfiltered and filtered magnetic anomalies of each segment to get the respective depth sections to the top and bottom of the oceanic crust. The same procedure is carried out for all gravity profiles which are sub-divided into various segments, as shown in Tables 2, 4, 6, 8, and 10. Each segment and its filtered (0.08 Hz) components are subjected to the spectral method to get the basement and deeper depths of the oceanic crust.

2D seismic lines were acquired for regional-scale exploration in the deep-water Mahanadi offshore to decipher the signature of the 85°E ridge and to understand the causes for its emplacement (Bastia et al. 2010). High amplitude magnetic anomalies are observed over the gravity low of the 85°E ridge and their identifications suggest that the ridge traverses crust of varying ages (Desa et al. 2018). The Comorin Ridge has an average topography of around 500–1000 m concerning the surrounding ocean floor with maximum relief in the central part (Rao & Singh 2020). A clear understanding of the underlying subsurface structure connected to the northern part of the 85°E ridge is intricate due to the masking effect of continental margin-related features of the East Coast of India (Rao & Radhakrishna 2014).

The most salient feature in the geoid map of the northern Indian Ocean is the Indian Ocean Geoid Low, which appears like a very long wavelength feature of greater than 5000 km. It covers the entire Indian Ocean and the origin of IOGL is still not clearly understood (Sreejith et al. 2013). A three-dimensional (3D) flexural modelling and coherence analysis of satellite-derived gravity and bathymetry data along the ridge were carried out to understand the mode of emplacement of Chagos-Laccadive Ridge (CLR) and the nature of the underlying crust (Sreejith et al. 2019). The process-oriented modelling uses gravity anomaly data and is an extremely useful technique to investigate geologically complex regions, where the gravity anomalies have changed through geological ages (Sreejith et al. 2011).

In general, the 85°E ridge is associated with significant magnetic anomalies compared to the anomalies of the oceanic crust in the Bay of Bengal (Liu et al. 1983, Ramana et al. 1997, Rao et al. 1997). The overall strength of the magnetization of the 85°E ridge suggests that the ridge is made of highly magnetized rocks. The asymmetry in the magnetic anomaly is attributed to the phase shift produced by the northward drift of the Indian plate (Liu et al. 1983). A recent compilation of geophysical data over the north-eastern Indian Ocean (Krishna et al. 2009, Michael & Krishna 2011) revealed alternative stripes of high amplitude positive and negative magnetic anomalies along the 85°E ridge track in the Bay of Bengal region. Michael & Krishna (2011) have correlated these magnetization patterns to a geomagnetic time scale and assigned approximate ages to the ridge track.

Profile-1 (1°N, 77°E–90°E)

For the magnetic anomaly profile, the depths to the top of the basement vary in the range of 3–8.8 km for the spectral technique and 4–8 km in the case of the Werner technique. The bottom depths from the spectral technique and Werner technique vary in the range of 6.7–12.8 km and 9–14 km range respectively (Tab. 1). For the free-air anomaly profile, the depths to the basement vary in the range of 6.1–7.9 km and deeper depths have a variation of 8.46–11.1 km as shown in Table 2. The interpreted depths from 2D gravity modelling almost correlated with the spectral depths obtained from gravity data (Tab. 2). The spectral and Werner depths, thus obtained from both magnetic and gravity data (only spectral) are used to draw a tentative model of the oceanic crust as shown in Figure 7. These depths when

plotted show undulations of oceanic crust and it can be observed that the thickness of the crust deciphered from gravity is thin when compared to crustal thickness obtained from magnetic data.

Table 1
Spectral and Werner depths along profile-1 (1°N, 77°E–90°E, length: 1442 km)

Magnetic profile results					
Segment	**Segment length [km]**	**Spectral depths [km]**		**Werner depths [km]**	
		unfiltered (Z_1)	**filtered (Z_2)**	**unfiltered (Z_1)**	**filtered (Z_2)**
MP 1-1	0–97	3.0	6.7	4.0	9.0
MP 1-2	90–387	6.61	9.7	7.0	11.0
MP 1-3	374–708	8.8	11.1	9.0	12.0
MP 1-4	699–1442	7.73	12.8	8.0	14.0

Table 2
Spectral depths along profile-1 (1°N, 77°E–90°E, length: 1442 km)

Free-air anomaly profile results					
Segment	**Segment length [km]**	**Spectral depths [km]**		**2D gravity modelling**	
		filtered (Z_1)	**filtered (Z_2)**	**upper crustal depth [km]**	**lower crustal depth [km]**
GP 1-1	0–520	6.1	11.1	6.0	9.0
GP 1-2	510–834	7.89	10.0	7.0	8.5
GP 1-3	820–1248	7.0	9.7	6.3	8.0
GP 1-4	1240–1442	6.1	8.46	4.0	9.0

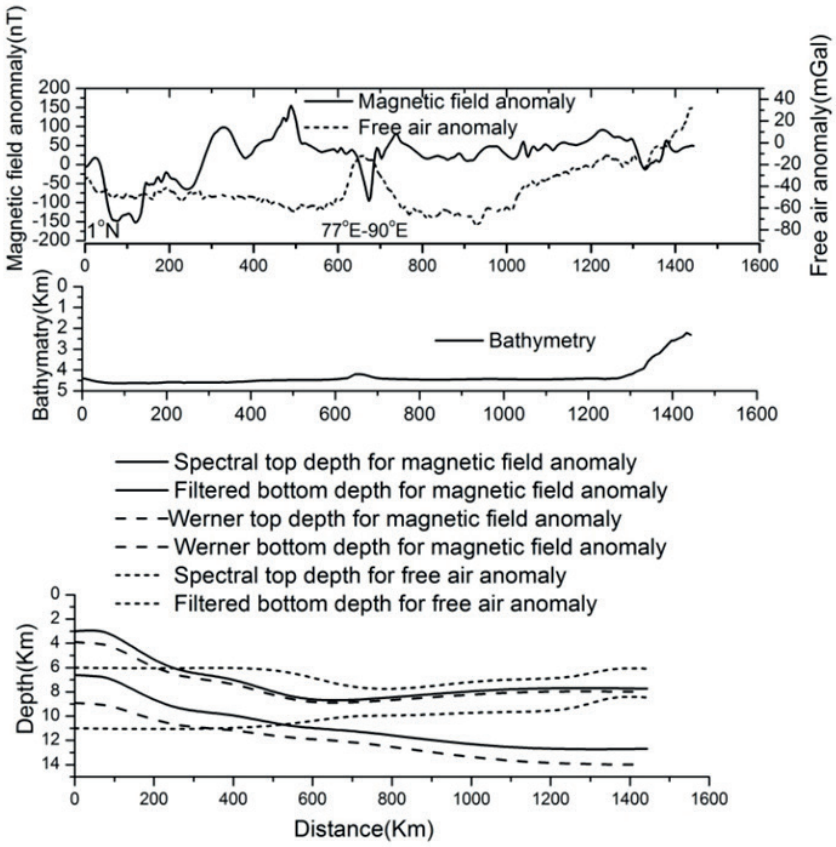

Fig. 7. *Combined depth model of magnetic and free-air anomaly along profile-1*

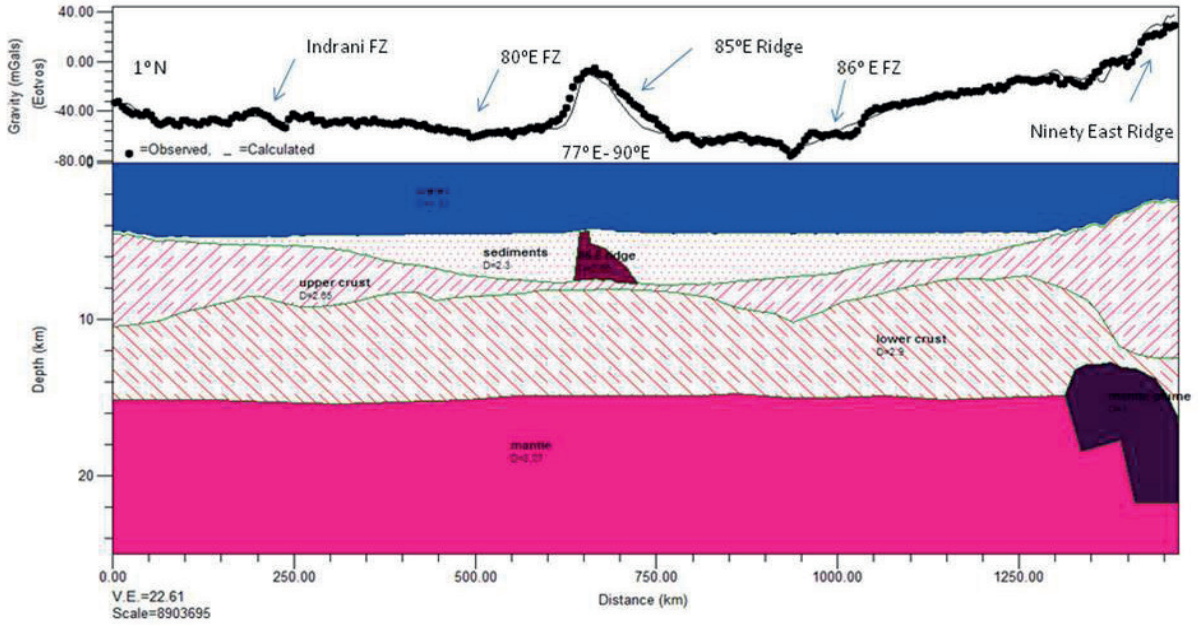

Fig. 8. *2D gravity model along profile-1 (1°N, 77°E–90°E)*

The bathymetry corresponding to the free-air anomaly profile-1 (1°N, 77°E–90°E) shown in Figure 8 gradually decreases in an easterly direction and to a minimum (nearly 2500 m) at the 90°E ridge. The sediment thickness gradually increases in an easterly direction and reaches the minimum at the 85°E ridge. The lower crustal thickness varies 4–5 km and has a density of 2.9 gm/cm^3. The NER is elevated by 2–3 km concerning neighbouring Bengal Fan sediments and shows a gravity high of about 28 mGal. The density of mantle plumes is 3 gm/cm^3 and thickness varies 2–6 km. Thus, the deformations produce intraplate seismicity along NER with a greater magnitude which pull out within the Indian plate.

Profile-2 (2°N, 77°E–90°E)

This profile is along the W-E direction with 2°N latitude and between 77°E–90°E longitudes. The spectral analysis yields depths to the shallow and deeper layers in the range of 4.86–6.64 km and 8.89–15.5 km respectively. The depths determined from the Werner deconvolution are in the range of 5–6.5 km and 9–15 km respectively to shallow and deeper layers and depth values are shown in Table 3. For the gravity profile, the depths to the basement vary in the range of 4.5–6 km and deeper depths show the variation of 7.3–11.7 km (Tab. 4).

Table 3
Spectral and Werner depths along profile-2 (2°N, 77°E–90°E, length: 1442 km)

Magnetic profile results					
Segment	**Segment length [km]**	**Spectral depths [km]**		**Werner depths [km]**	
		unfiltered (Z_1)	**filtered (Z_2)**	**unfiltered (Z_1)**	**filtered (Z_2)**
MP 2-1	0–205	5.64	10.47	6.0	11.0
MP 2-2	181–316	6.2	8.89	5.0	9.0
MP 2-3	310–439	6.24	15.54	6.0	15.0
MP 2-4	430–681	6.64	11.39	6.5	11.0
MP 2-5	675–1442	4.86	14.6	5.0	15.0

Table 4
Spectral depths along profile-2 (2°N, 77°E–90°E, length: 1442 km)

Free-air anomaly profile results					
Segment	**Segment length [km]**	**Spectral depths [km]**		**2D gravity modelling**	
		unfiltered (Z_1)	**filtered (Z_2)**	**upper crustal depth [km]**	**lower crustal depth [km]**
GP 2-1	0–214	4.7	7.3	4.3	9.0
GP 2-2	210–394	4.5	8.8	5.5	10.0
GP 2-3	385–724	6.0	7.3	6.9	9.5
GP 2-4	715–926	4.75	8.0	6.5	10.0
GP 2-5	915–1205	4.79	8.9	6.2	8.5
GP 2-6	1190–1442	5.58	11.7	4.5	12.5

The depths to the top and bottom of each anomaly segment obtained from these two techniques have shown undulations that can be observed from a tentative model of the oceanic crust (Fig. 9). The thickness of the crust deciphered from gravity is thin and shallow when compared to crustal thickness obtained from magnetic data.

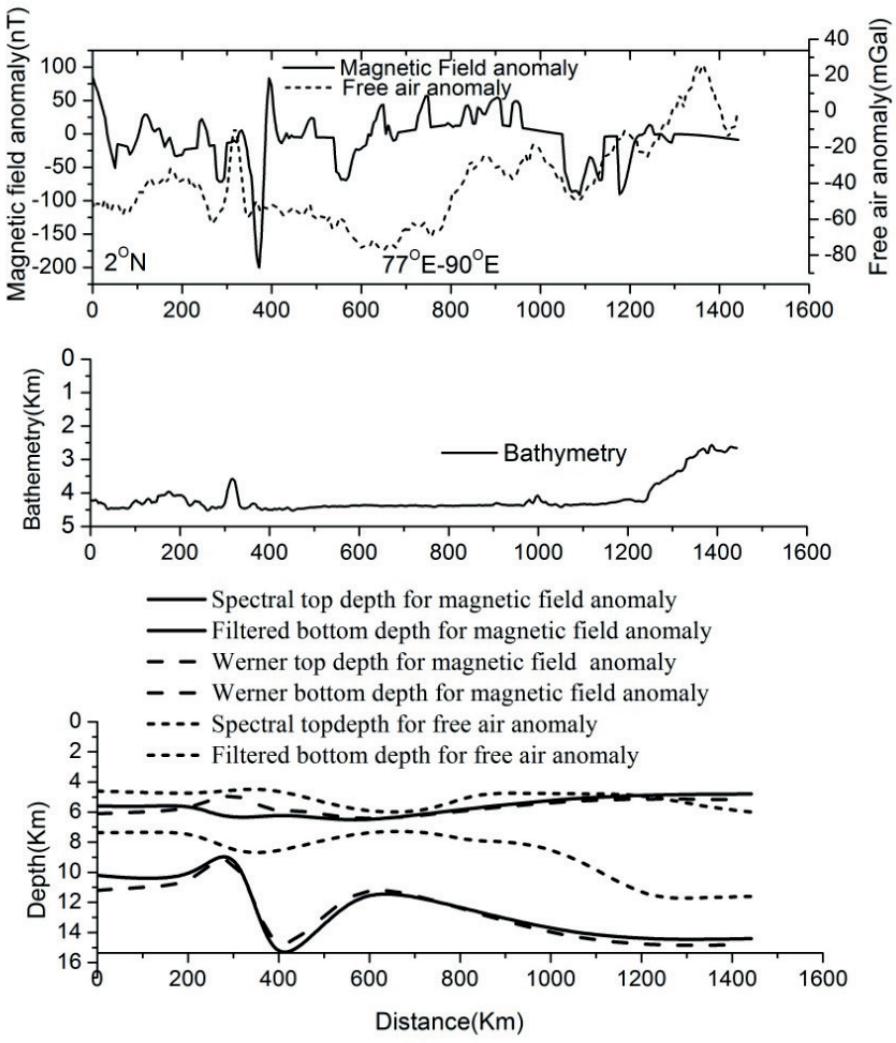

Fig. 9. *Combined depth model of magnetic and free-air anomaly along profile-2*

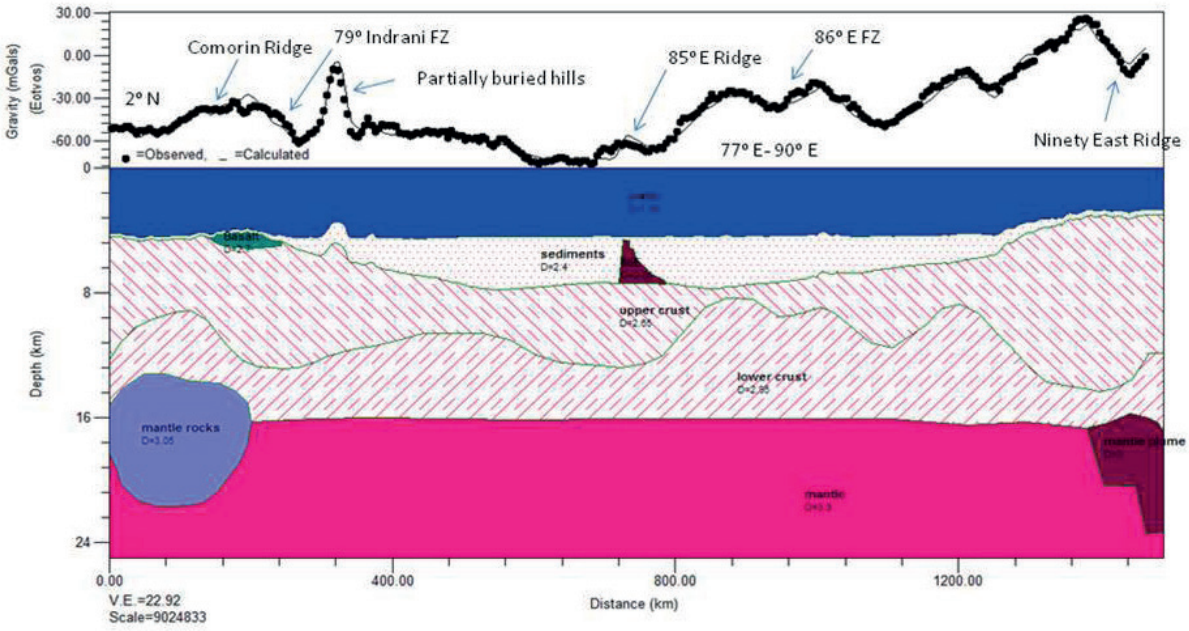

Fig. 10. *2D gravity model along profile-2 (2°N, 77°E–90°E)*

The bathymetry corresponding free-air anomaly profile-2 in Figure 10 gradually decreases in an easterly direction and to a minimum (2600 m nearly) at the 90°E ridge. The sediments thickness is negligible corresponding to the Comorin Ridge and gradually increases in an easterly direction. It reaches a minimum at the 85°E ridge but sediment thickness increases on both sides of ridge. The average depth of the 85°E ridge is nearly 6 km and the width of the ridge is nearly 62 km. A gravity high of –10 mGal is observed at a distance of 322 km due to tectonic features like buried seamounts. The upper crust is thin with undulations apart from at the Comorin and Ninety East ridges. The average crustal thickness at the Comorin and Ninety East ridges is nearly 8–10 km.

The lower crust has a crustal thickness that varies up to 6 km and its density is nearly 2.9 gm/cm^3. The NER is elevated by 1–2 km for the neighbouring Bengal Fan sediments of the oceanic crust which shows a gravity high of about 26 mGal. The density of the mantle plumes due to hotspot activity is 3 gm/cm^3 and thickness varies 2–6 km which suggests a cushion-like structure. The density of mantle rocks is 3.05 gm/cm^3 associated with the Comorin Ridge and basaltic rocks (2.7 gm/cm^3) below the sediment layer. The Indian plate may have deformations that produce large magnitude intraplate seismicity along the NER.

Profile-3 (3°N, 77°E–90°E)

This magnetic profile runs in a W-E direction with 3°N latitude and between 77°E–90°E longitudes. The top depths of the oceanic basement have been determined as shown in Table 5 within the range of 2.56–9.16 km and bottom depths (Curie isotherm) vary in the range of 8.3–13 km. The Werner deconvolution technique was applied for the unfiltered and filtered magnetic anomalies of each segment to obtain the respective depth sections of the oceanic crust. The depths to the top of the basement vary in the range of 3–9 km and the bottom depths have a variation of 10–15 km (Tab. 5). These two (spectral and Werner) depth sections are in good agreement.

The gravity profile is divided into six segments based on the anomaly pattern as shown in Table 6, with depths to the basement varying in the range of 3.7–8 km while deeper depths show a variation of 8.35–15 km which shows undulations in the oceanic crust. A tentative crustal model of the oceanic crust is constructed based on crustal

depths derived from gravity and magnetic data as shown in Figure 11. These depths when plotted in Figure 11 show undulations of the oceanic crust which indicates deformations. The thickness of the crust deciphered from gravity and magnetic data are more or less equal.

Table 5
Spectral and Werner depths along profile-3 (3°N, 77°E– 90°E, length: 1442 km)

Magnetic profile results					
Segment	**Segment length [km]**	**Spectral depths [km]**		**Werner depths [km]**	
		unfiltered (Z_1)	**filtered (Z_2)**	**unfiltered (Z_1)**	**filtered (Z_2)**
MP 3-1	0–200	4.75	8.72	6.0	10.0
MP 3-2	190–331	7.46	10.0	7.0	11.0
MP 3-3	320–423	9.16	15.0	9.0	14.0
MP 3-4	415–532	5.0	8.35	4.0	10.0
MP 3-5	525–623	7.0	12.2	8.0	12.0
MP 3-6	608–773	8.54	13.0	9.0	14.0
MP 3-7	760–950	7.7	11.6	9.0	13.0
MP 3-8	940–1116	6.8	11.1	8.0	12.0
MP 3-9	1110–1199	2.56	14.0	3.0	15.0
MP 3-10	1190–1290	8.5	15.0	8.0	14.0
MP 3-11	1280–1442	5.8	11.0	6.0	10.0

Table 6
Spectral depths along profile-3 (3°N, 77°E– 90°E, length: 1442 km)

Free-air anomaly profile results					
Segment	**Segment length [km]**	**Spectral depths [km]**		**2D gravity modelling**	
		unfiltered (Z_1)	**filtered (Z_2)**	**upper crustal depth [km]**	**lower crustal depth [km]**
GP 3-1	0–188	3.7	8.35	4.1	10.0
GP 3-2	180–436	7.9	11.0	6.0	9.0
GP 3-3	430–745	6.1	10.0	6.6	8.0
GP 3-4	740–995	8.0	10.3	7.0	9.0
GP 3-5	990–1243	6.3	13.0	5.5	10.5
GP 3-6	1235–1442	4.5	12.0	4.0	11.0

The bathymetry corresponding to free-air anomaly profile-3 (3°N, 77°E–90°E) as shown in Figure 12 gradually decreases in an easterly direction and reaches the minimum (nearly 1460 m) at the 90°E ridge. The sediments thickness is more or less uniform and becomes the minimum at the 85°E ridge. The crest of the ridge has negligible sediment thickness and increases on either side, but the sediment load flattens the flanks deviation caused by the ridge load. The upper crust is thin, with an average thickness is nearly 2–3 km, except at the Comorin and Ninety East ridges. The density of the upper crust is nearly 2.65 gm/cm^3 and extremely thin (2.5 km) at the 85°E ridge. The lower crustal thickness varies 2–5 km and has a density of 2.9 gm/cm^3.

The density of the mantle plumes is 3 gm/cm^3 with a variable thickness of 2–4 km. The magmatic rocks with a density of 3.05 gm/cm^3 correspond to the negative anomaly of the Comorin Ridge which causes deformations to extend within the Indian Ocean plate.

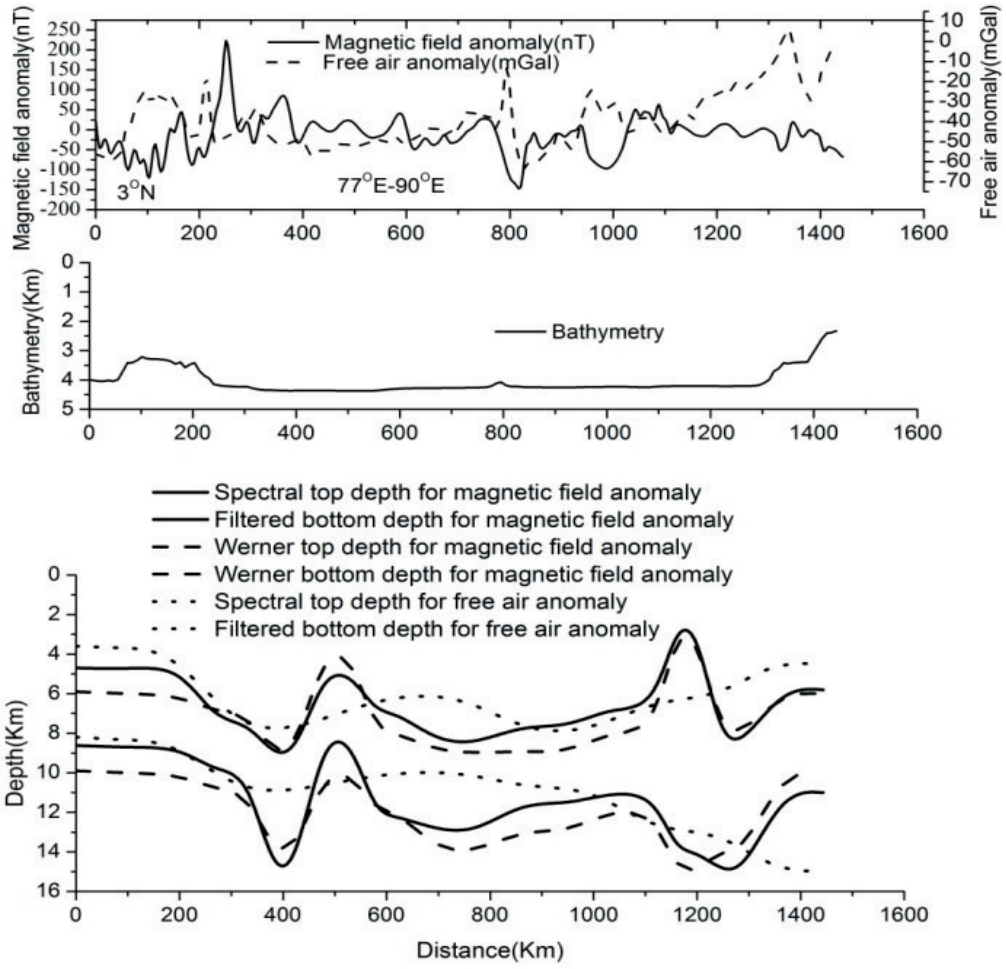

Fig. 11. *Combined depth model of magnetic and free-air anomaly along profile-3*

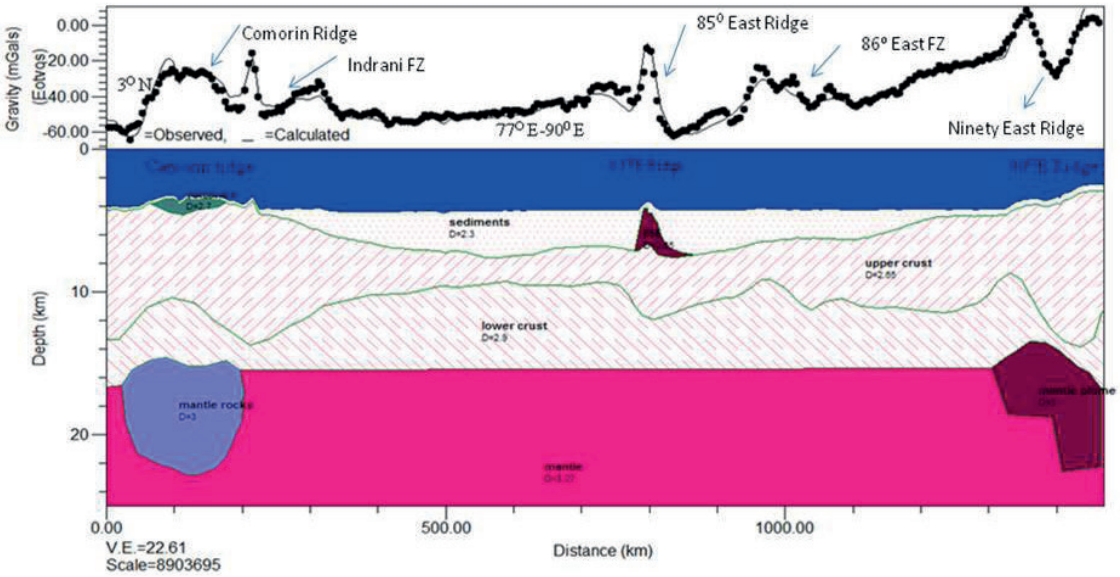

Fig. 12. *2D gravity model along profile-3 (3°N, 77°E–90°E)*

Profile-4 (4°N, 77°E–90°E)

This profile runs in a W-E direction along 4°N latitude and between 77°E–90°E longitudes and is divided into seven segments. The spectral and Werner depth values of the magnetic anomaly profile are shown in Table 7. The depths to the top of the basement vary in the range of 4.77–7.63 km in respect of the spectral technique and 3–8 km for the Werner technique. The bottom depths from the spectral technique vary in the range of 7–11.8 km, whereas Werner depth shows a 9–11 km range (Tab. 7). The spectral and Werner depths obtained from magnetic data corresponding to the top and bottom of oceanic crust are in the same range.

For the gravity profile, the depths to the basement vary in the range of 5–7.3 km while deeper depths show a variation of 9–12.5 km (Tab. 8). The spectral and Werner depths obtained from both magnetic and gravity (only spectral) have been used to draw a tentative model of the oceanic crust showing undulations (Fig. 13). The crustal depths of the oceanic crust obtained from gravity data and the interpreted crustal depths from 2D gravity modelling (Tab. 8) are in good agreement.

Table 7
Spectral and Werner depths along profile-4 (4°N, 77°E–90°E, length: 1442 km)

Magnetic profile results					
Segment	**Segment length [km]**	**Spectral depths [km]**		**Werner depths [km]**	
		unfiltered (Z_1)	**filtered (Z_2)**	**unfiltered (Z_1)**	**filtered (Z_2)**
MP 4-1	0–90	5.96	8.46	6.0	10.0
MP 4-2	85–178	5.41	9.55	4.0	10.0
MP 4-3	170–398	5.23	7.05	4.0	9.0
MP 4-4	390–759	4.77	9.02	4.0	8.5
MP 4-5	750–929	5.93	7.95	4.5	9.0
MP 4-6	920–1180	7.46	11.8	8.0	11.0
MP 4-7	1175–1442	7.63	10.25	7.0	10.8

Table 8
Spectral depths along profile-4 (4°N, 77°E–90°E, length: 1442 km)

free-air anomaly profile results					
Segment	**Segment length [km]**	**Spectral depths [km]**		**2D gravity modelling**	
		unfiltered (Z_1)	**filtered (Z_2)**	**upper crustal depth [km]**	**lower crustal depth [km]**
GP 4-1	0–295	6.3	10.3	5.0	9.5
GP 4-2	285–844	5.1	9.0	6.2	8.0
GP 4-3	830–956	7.3	11.1	6.8	9.5
GP 4-4	950–1163	7.0	11.5	5.5	10.0
GP 4-5	1150–1442	5.0	11.0	4.5	9.6

The bathymetry corresponding to the free-air anomaly profile as shown in Figure 14 is nearly 4 km at the Comorin Ridge and gradually increases in an easterly direction. The bathymetry is almost at the minimum (3300 m nearly) at the 90°E ridge. The sediments thickness is at the minimum at the Comorin Ridge and the 90°E ridge. The sediments have a density of 2.3 gm/cm^3 and sediments thickness is negligible above the crest of the 85°E ridge and elevates on either side due to partially buried hills. The ridge load creates a deflection of the flanks, which are finally flattened by sediment load.

The upper crust is thin except at the Comorin, 85°E, and 90°E ridges. The density of the upper crust is nearly 2.65 gm/cm^3 and extremely thin between the Comorin and 85°E ridges. The lower crustal thickness varies 2–6 km and has a density of 2.9 gm/cm^3. The NER is elevated from 1–2 km for adjoining Bengal Fan sediments. The compensatory mass underlying the NER suggests hot spot activity from gravity modelling.

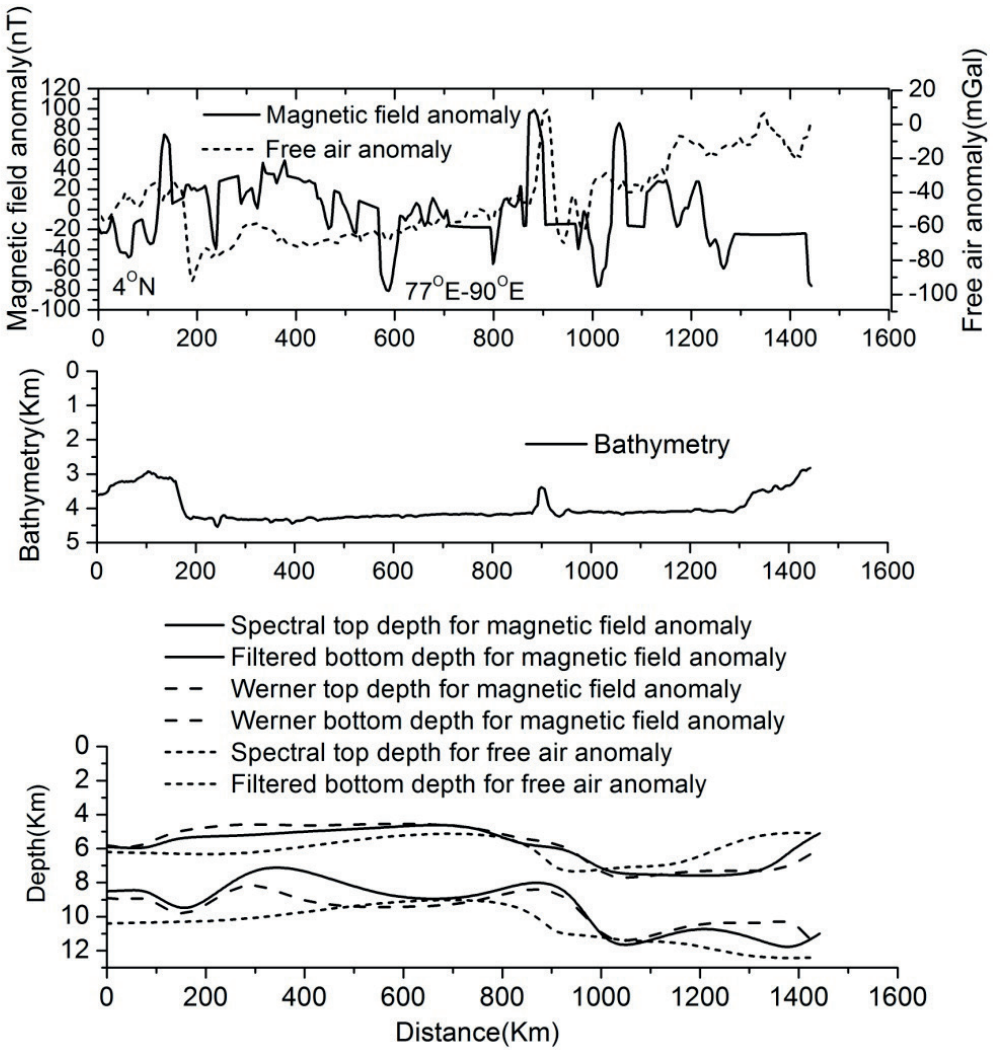

Fig. 13. *Combined depth model of magnetic and free-air anomaly along profile-4*

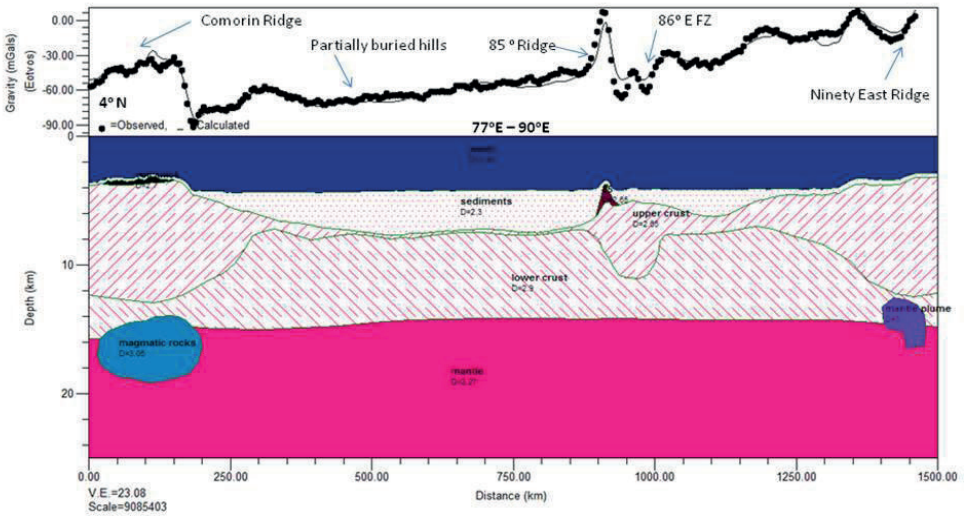

Fig. 14. *2D gravity model along profile-4 (4°N, 77°E–90°E)*

The density of the mantle plumes is 3 gm/cm^3 with thickness varies 2–4 km. The mantle consists of magmatic rocks having a density of 3.05 gm/cm^3 corresponding negative anomaly (–34 mGal) of the Comorin Ridge. Thus, the large magnitude intraplate seismicity along the NER is produced within the Indian Ocean plate due to deformations. The average thickness of sediments above the 90°E ridge is nearly 500 m and is primarily composed of sub-alkaline basalt rocks. Most of the sediments on the Ninety East Ridge are categorized as pelagic, so it can be understood that the rate of sediment build-up on the ridge has been slower than in other parts of the ocean.

Profile-5 (5°N, 77°E–90°E)

This profile runs in a W-E direction along 5°N latitude and between 77°E–90°E longitudes. The crustal depths at the top of the basement vary in the range of 4.8–9 km in respect of the spectral technique and 6–10 km for the Werner technique. The bottom depths from the spectral technique vary in the range of 8.5–15 km, whereas Werner depth shows a 10–15 km range (Tab. 9).

For the gravity profile, the depths to the basement vary in the range of 5–9 km while deeper depths show a variation of 7–12 km as shown in Table 10. The spectral and Werner depths obtained from both magnetic and gravity data (only spectral) are used to draw a tentative model of the oceanic crust as shown in Figure 15. The thickness of the crust deciphered from gravity is thin and shallow when compared to the thickness obtained from magnetic data.

The free-air anomaly profile-5 (5°N, 77°E–90°E) corresponding bathymetry is at the minimum at the Comorin Ridge as shown in Figure 16 and increases in an easterly direction. The sediments thickness is at the minimum at the Comorin Ridge and gradually increases in an easterly direction. The sediments thickness is negligible on the 85°E ridge crest and rises on either side. The sediment load flattens the flanks of the deflection which is caused by the ridge load. The upper crust is extremely thin in between the Comorin and 85°E ridges. The lower crustal thickness varies 2–6 km and has a density of 2.9 gm/cm^3. The NER is elevated 1–2 km for nearby Bengal Fan sediments.

Table 9
Spectral and Werner depths along profile-5 (5°N, 77°E–90°E, length: 1442 km)

Magnetic profile results					
Segment	**Segment length [km]**	**Spectral depths [km]**		**Werner depths [km]**	
		unfiltered (Z_1)	**filtered (Z_2)**	**unfiltered (Z_1)**	**filtered (Z_2)**
MP 5-1	0–196	5.3	12.7	7.0	14.0
MP 5-2	190–706	9.0	15.0	10.0	14.0
MP 5-3	700–813	4.8	8.5	6.0	10.0
MP 5-4	808–961	9.0	14.0	8.0	15.0
MP 5-5	954–1106	7.0	11.0	6.0	12.0
MP 5-6	1100–1442	8.0	13.4	9.0	14.0

Table 10
Spectral depths along profile-5 (5°N, 77°E-90°E, length: 1442 km)

Free-air anomaly profile results					
Segment	**Segment length [km]**	**Spectral depths [km]**		**2D gravity modelling**	
		unfiltered (Z_1)	**filtered (Z_2)**	**upper crustal depth [km]**	**lower crustal depth [km]**
GP 5-1	0–185	7.0	9.7	5.0	11.5
GP 5-2	180–485	5.8	9.0	6.0	10.5
GP 5-3	480–770	7.0	11.0	7.2	9.5
GP 5-4	764–902	5.0	7.0	6.0	8.0
GP 5-5	895–1057	9.0	12.0	7.0	11.0
GP 5-6	1050–1234	5.3	10.3	5.0	9.5
GP 5-7	1230–1442	5.0	9.4	4.0	8.5

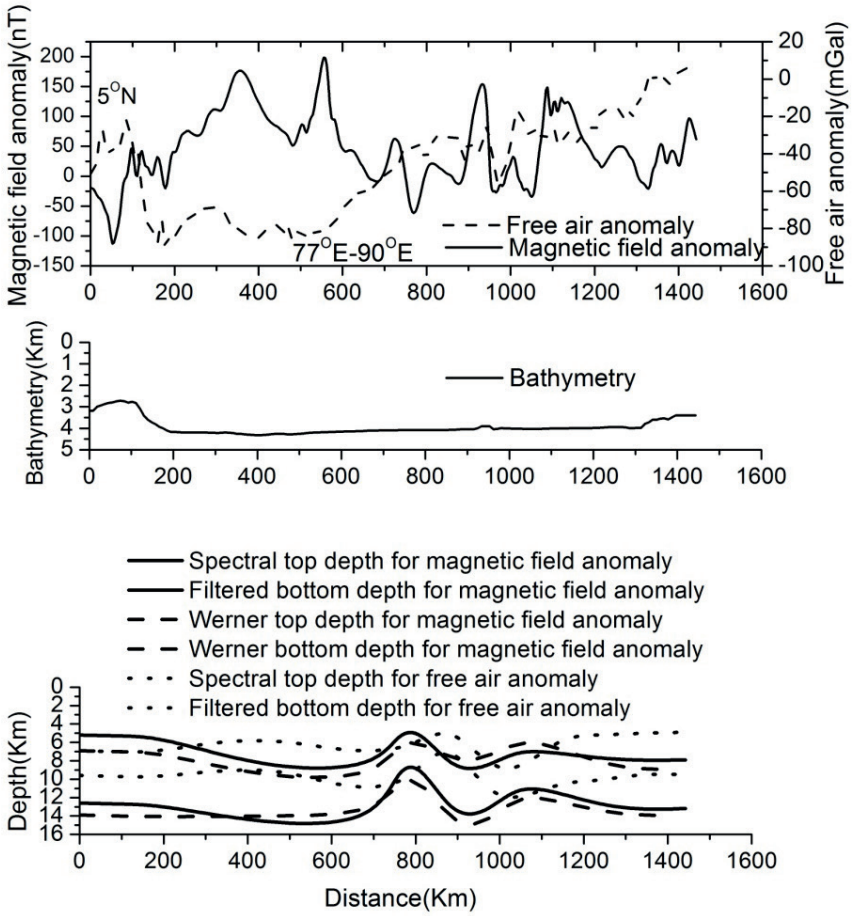

Fig. 15. *Combined depth model of magnetic and free-air anomaly along profile-5*

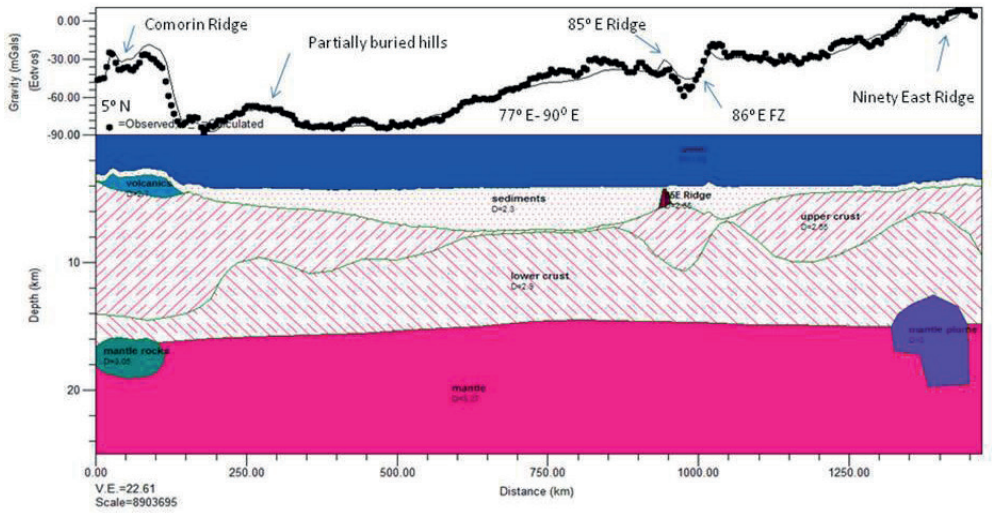

Fig. 16. *2D gravity model along profile-5 (5°N, 77°E–90°E)*

The density of the mantle plumes is 3.0 gm/cm^3 and thickness varies 3–4 km. The mantle consists of magmatic rocks having a density of 3.05 gm/cm^3 corresponding negative anomaly (–40 mGal) of the Comorin Ridge. Therefore, the deformations lengthen within the Indian Ocean plate which

may produce bulk magnitude intraplate seismicity along the NER. The average sediment thickness is negligible above the 90°E ridge and is composed of sub-alkaline basalt rocks.

CONCLUSIONS

The gravity and magnetic data south of Sri Lanka covering the area between 1°N–5°N and 77°E–90°E has been subjected to a preliminary interpretation by means of the spectral and Werner deconvolution techniques. These two techniques yield approximate depths for the oceanic crust. The plot of these depths along the profiles in the W-E direction with a 1° interval shows the crustal structure of the study area. The depth structures along the profiles are shown in Figures 7, 9, 11, 13, and 15. From the analysis of these tentative crustal models derived from gravity data with supporting 2D gravity modelling results for the same profiles, one can easily decipher that the depths to the basement and its bottom undulate along with the profiles. This indicates that the oceanic crust might have undergone deformation as suggested by numerous authors of seismic studies. The significant finding is that the depths obtained from the spectral and Werner techniques of magnetic data have yielded nearly the same results, thus reducing ambiguity. The average top depth of the oceanic crust varies in the range of 4–10 km whereas the bottom depths are in the range of 7–15 km. The oceanic crustal thickness varies between 3.4 km and maximum up to 9 km. The 2D gravity models (Figs. 8, 10, 12, 14, 16) show the deformation of the oceanic crust due to tectonic features like ridges and fracture zones. From an integrated interpretation of the longitudinal fracture zones, sea-floor topography, gravity, and seismic data, deformed crustal blocks have been identified by Rao et al. (2004). This supports the deformation of the oceanic crust of this region as suggested by numerous scientists working in this area.

Crustal thickness contour maps were prepared from the depths determined for magnetic data from spectral and Werner methods. Similarly, for free-air gravity data, a crustal thickness contour map was prepared from the depths determined from the spectral method. The crustal thickness varies in the range of 1.5–11 km. The maximum thickness of 11 km is observed at approximately 3°N and 87°E (Figs. 17, 18). From the crustal thickness of gravity data, the maximum thickness of 11km is observed at approximately 3°N and 89°E positions (Fig. 19), and the contour trend here is in the W-E direction whereas, in the case of magnetic data, the trend is in the N-S direction. There is a good correlation between the crustal thickness maps of the spectral and Werner techniques of magnetic data. The thickness of the crust derived from gravity data is relatively thin and shallow which is correlated with 2D gravity models (Figs. 8, 10, 12, 14, 16). The contour closures of varying thicknesses were observed on the three maps (Figs. 17–19) which indicate the intensive deformation of the crust.

From the interpreted 2D gravity models, the average depth of the 85°E ridge is nearly 7.6 km and the width is nearly 100 km. The ridge is completely buried under the sediments and has a density of 2.65 gm/cm^3 with sediments of a density of 2.3 gm/cm^3. It is observed that sediment thickness is almost negligible above the crest of the ridge and accelerates on either side. The upper crust is thin and has an average thickness that varies up to 6 km except at the Ninety East Ridge. The average crustal thickness is at the maximum (10–12 km) at the Ninety East Ridge. The density of the upper crust is nearly 2.65 gm/cm^3 and extremely thin at 85°E ridge. The NER is interpreted using a 2D forward gravity model using existing seismic constraints that suggest hot spot activity. The density of the mantle is 3.27 gm/cm^3 and has a compensation mechanism of NER. The 2D gravity model results suggest that the crust beneath the southern part of the Comorin Ridge consists of 2 km thick volcanic rocks, 6–7 km thick oceanic crust, and 6–8 km thick underplated magmatic rocks.

The seismic refraction data of the southern part of BOB is available between 0°N to 10°N and was collected from ocean bottom seismometer readings obtained from Russian surveys (Subrahmanyam & Singh 1992). The computed velocities for the sediments are 2–5.7 km/s and 6.1–7.7 km/s for the oceanic igneous layer and 8.3–8.5 km/s for the oceanic upper mantle. The seismic velocities were used to determine the densities of oceanic crust with the velocity-density relationship (Christensen 1982). The 85°E ridge is modelled using seismic data which determines the elastic plate thickness.

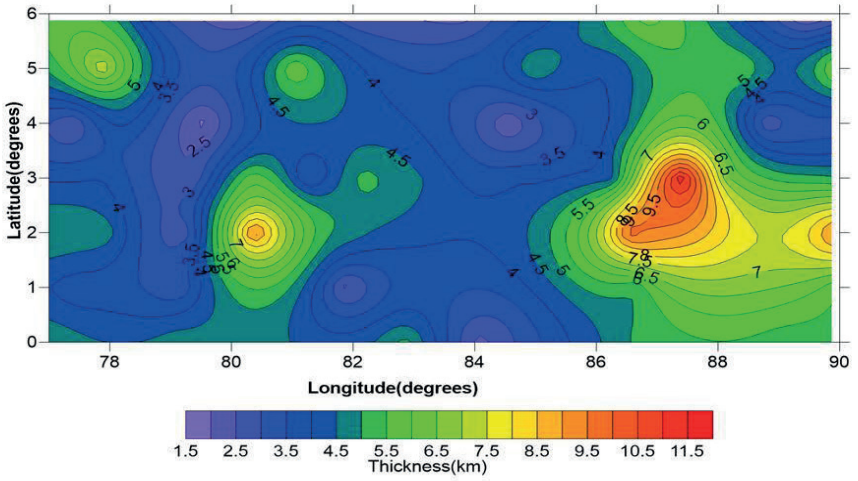

Fig. 17. *Crustal thickness contour map obtained for the magnetic data from the spectral method*

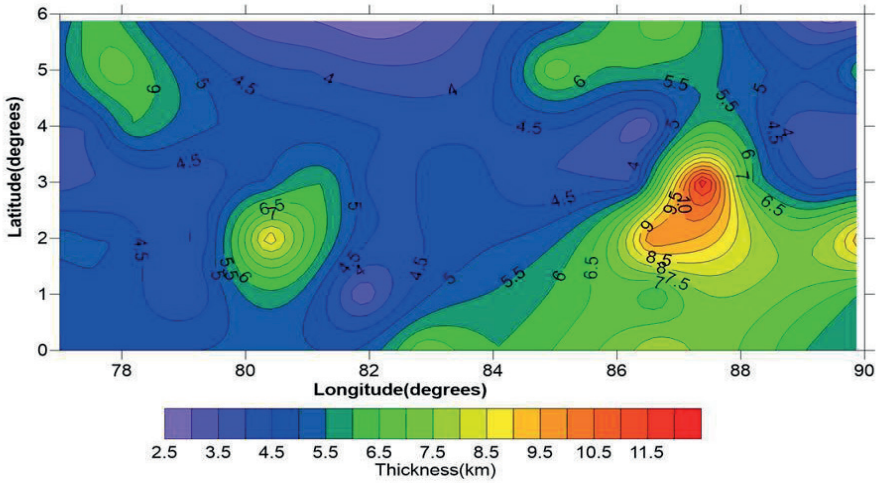

Fig. 18. *Crustal thickness contour map obtained for the magnetic data from the Werner method*

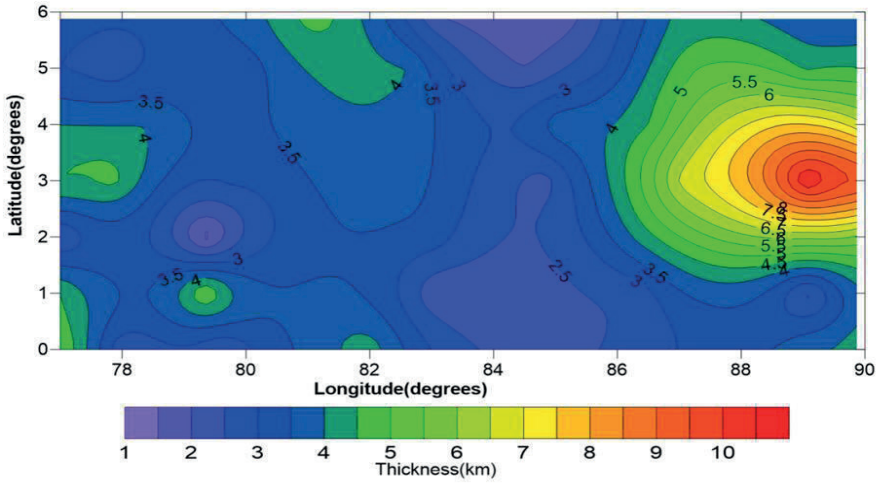

Fig. 19. *Crustal thickness contour map obtained for the free-air gravity data from the spectral method*

The elastic plate thickness varies 10–15 km for both northern and southern parts of the ridge. This suggests that the ridge is emplaced in an intraplate setting. The average thickness of the 85°E ridge is nearly 5 km with a density of 2.65 gm/cm^3 (Sreejith et al. 2011). The isostatic compensation of the Comorin Ridge suggests that the crust beneath the southern part of the ridge is nearly 17 km thick which consists of 2 km thick volcanic rocks, 6 km thick oceanic crust, and 9 km thick underplated magmatic rocks (Sreejith et al. 2008). The average crustal thickness is maximum up to 10–12 km at Ninety East Ridge and again decreases towards the Nicobar Fan. The NER gravity field is interpreted with isostatic compensation by using existing seismic constraints which suggests hot spot activity. The density of the mantle is 3.27 gm/cm^3 and has hot spot activity which suggests a compensation mechanism of the NER (Mukhopadhyay & Krishna 1995).

The author conveys his sincere thanks to the anonymous reviewers for their constructive suggestions in improving the quality of the paper.

The author declares that he has no conflict of interest and adheres to copyright norms.

REFERENCES

Amante C. & Eakins B.W., 2009. *ETOPO1 1 arc- minute global relief model: procedures, data sources and analysis*. NOAA Technical Memorandum NESDIS NGDC-24. https://doi.org/10.7289/V5C8276M.

Bastia R., Radhakrishna M., Das S., Kale A.S. & Catuneanu O., 2010. Delineation of the 85 E ridge and its structure in the Mahanadi Offshore Basin, Eastern Continental Margin of India (ECMI), from seismic reflection imaging. *Marine and Petroleum Geology*, 27(9), 1841–1848. https://doi.org/10.1016/j.marpetgeo.2010.08.003.

Bull J.M. & Scrutton R.A., 1990. Fault reactivation in the central Indian Ocean and the rheology of oceanic lithosphere. *Nature*, 344(6269), 855–858. https://doi.org/10.1038/344855a0.

Bull J.M., Martinod J. & Davy P., 1992. Buckling of the oceanic lithosphere from geophysical data and experiments. *Tectonics*, 11, 537–548. http://doi.org/10.1029/91TC02908.

Curray J.R. & Moore D.G., 1971. Growth of the Bengal deep-sea fan and denudation in the Himalayas. *Geological Society of America Bulletin*, 82(3), 563–572. https://doi.org/10.1130/0016-7606(1971)82[563:GOTBDF]2.0.CO;2.

Curray J.R., Emmel F.J., Moore D.G. & Raitt R.W., 1982. Structure, Tectonics, and Geological History of the Northeastern Indian Ocean. [in:] Nairn A.E.M. & Stehli F.G. (eds.), *The Ocean Basins and Margins*, Springer, Boston, MA, 399–450. https://doi.org/10.1007/978-1-4615-8038-6_9.

Christensen N.I., 1982. Seismic Velocities. [in:] Carmichael R.S. (ed.), *Handbook of Physical Properties of Rocks. Volume II*, CRC Press, Boca Raton, 1–228.

Curray J.R. & Munasinghe T., 1991. Origin of the Rajmahal Traps and the 85 E ridge: Preliminary reconstructions of the trace of the Crozet hotspot. *Geology*, 19(12), 1237–1240. https://doi.org/10.1130/0091-7613(1991)019<1237:OOTRTA>2.3.CO;2.

Desa M.A., Ismaiel M., Suresh Y. & Krishna K.S., 2018. Oblique strike-slip motion of the Southeastern Continental Margin of India: Implication for the separation of Sri Lanka from India. *Journal of Asian Earth Sciences*, 156, 111–121. https://doi.org/10.1016/j.jseaes.2018.01.015.

Geller C.A., Weissel J.K. & Anderson R.N., 1983. Heat transfer and intraplate deformation in the central Indian Ocean. *Journal of Geophysical Research: Solid Earth*, 88(B2), 1018–1032. https://doi.org/10.1029/JB088iB02p01018.

Gopala Rao D., Krishna K.S., Neprochnov Yu.P. & Grinko B.N., 2004. Satellite gravity anomalies and crustal features of the Central Indian Ocean Basin. *Current Science*, 86(7), 948–957. http://www.jstor.org/stable/24109277.

Haxby W.F., 1987, *Gravity Field of the World's Oceans: A Portrayal of Gridded Geophysical Data Derived from GEOSAT Rader Altimeter Measurements of the Shape of the Ocean Surface*. Department of the US Navy, Office of Naval Research and NOAA Data Center, Boulder [map].

Kahle H.G., Naini B.R., Talwani M. & Eldholm O., 1981. Marine geophysical study of the Comorin ridge, north central Indian basin. *Journal of Geophysical Research: Solid Earth*, 86(B5), 3807–3814. https://doi.org/10.1029/JB086iB05p03807.

Krishna K.S., Ramana M.V., Rao D.G., Murthy K.S.R., Rao M.M., Subrahmanyam V. & Sarma K.V.L.N.S., 1998. Periodic deformation of oceanic crust in the central Indian Ocean. *Journal of Geophysical Research: Solid Earth*, 103(B8), 17859–17875. https://doi.org/10.1029/98JB00078.

Krishna K.S., Rao D.G. & Neprochnov Y.P., 2002. Formation of diapiric structure in the deformation zone, central Indian Ocean: A model from gravity and seismic reflection data. *Journal of Earth System Science*, 111(1), 17–28. https://doi.org/10.1007/ BF 02702219.

Krishna K.S., Michael L., Bhattacharyya R. & Majumdar T.J., 2009. Geoid and gravity anomaly data of conjugate regions of the Bay of Bengal and Enderby Basin: New constraints on breakup and early spreading history between India and Antarctica. *Journal of Geophysical Research: Solid Earth*, 114(B3). https://doi.org/10.1029/2008JB005808.

Liu C.S., Sandwell D.T. & Curray J.R., 1983. The negative gravity field over the 85 E Ridge. *Journal of Geophysical Research: Solid Earth*, 87(B9), 7673–7686. https://doi.org/10.1029/JB087iB09p07673.

Maus S. & Dimri V.P., 1994. Scaling properties of potential fields due to scaling sources. *Geophysical Research Letters*, 21(10), 891–894. https://doi.org/10.1029/94GL00771.

Maus S. & Dimri V., 1995. Potential field power spectrum inversion for scaling geology. *Journal of Geophysical Research: Solid Earth*, 100(B7), 12605–12616. https://doi.org/10.1029/95JB00758.

Maus S. & Dimri V., 1996. Depth estimation from the scaling power spectrum of potential fields? *Geophysical Journal International*, 124(1), 113–120. https://doi.org/10.1111/j.1365-246X.1996.tb06356.x.

Maus S., Barckhausen U., Berkenbosch H., Bournas N., Brozena J., Childers V., Dostaler F. et al., 2009. EMAG2: A 2-arcmin resolution Earth Magnetic Anomaly Grid compiled from satellite, airborne, and marine magnetic measurements. *Geochemistry, Geophysics, Geosystems*, 10(8), Q08005. https://doi.org/10.1029/2009GC002471.

Michael L. & Krishna K.S., 2011. Dating of the 85°E Ridge (northeastern Indian Ocean) using marine magnetic anomalies. *Current Science*, 100(9), 1314–1322. http://www.jstor.org/stable/24076596.

Mukhopadhyay M. & Krishna M.B.R., 1995. Gravity anomalies and deep structure of the Ninetyeast Ridge north of the equator, eastern Indian Ocean – a hot spot trace model. *Marine Geophysical Researches*, 17(2), 201–216. https://doi.org/10.1007/BF01203426.

Pilkington M., Gregotski M.E. & Todoeschuck J.P., 1994. Using fractal crustal magnetization models in magnetic interpretation. *Geophysical Prospecting*, 42(6), 677–692. https://doi.org/10.1111/j.1365-2478.1994.tb00235.x

Rabinowitz P.D. & LaBrecque J.L., 1977. The isostatic gravity anomaly: a key to the evolution of the ocean-continent boundary at passive continental margins. *Earth and Planetary Science Letters*, 35(1), 145–150. https://doi.org/10.1016/0012-821X(77)90037-1.

Radhakrishna M., Subrahmanyam C. & Damodharan T., 2010. The thin oceanic crust below Bay of Bengal inferred from 3-D gravity interpretation. *Tectonophysics*, 493(1–2), 93–105. https://doi.org/10.1016/j.tecto.2010.07.004.

Ramana M.V., Subrahmanyam V., Chaubey A.K., Ramprasad T., Sarma K.V.L.N.S., Krishna K.S. & Subrahmanyam C., 1997. Structure and origin of the 85 E Ridge. *Journal of Geophysical Research: Solid Earth*, 102(B8), 17995–18012. https://doi.org/10.1029/97JB00624.

Rao G.S. & Radhakrishna M., 2014. Crustal structure and nature of emplacement of the 85 E Ridge in the Mahanadi offshore based on constrained potential field modeling: Implications for intraplate plume emplaced volcanism. *Journal of Asian Earth Sciences*, 85, 80–96. https://doi.org/10.1016/j.jseaes.2014.01.026.

Rao G.S. & Singh A., 2020. Crustal architecture and isostatic compensation of the Comorin Ridge, central Indian Ocean: Implications for the breakup of east Gondwana. *Journal of Asian Earth Sciences*, 199, 104463. https://doi.org/10.1016/j.jseaes.2020.104463.

Rao D.G., Krishna K.S. & Sar D., 1997. Crustal evolution and sedimentation history of the Bay of Bengal since the Cretaceous. *Journal of Geophysical Research: Solid Earth*, 102(B8), 17747–17768. https://doi.org/10.1029/96JB01339.

Ravi Kumar S. & Subrahmanyam M., 2020. A tentative crustal model of the central Indian Ocean South of Srilanka as inferred from gravity and magnetic data. *Journal of Indian Geophysical Union*, 24(1), 27–42.

Royer J.Y. & Chang T., 1991. Evidence for relative motions between the Indian and Australian Plates during the last 20 m.y. from plate tectonic reconstructions: Implications for the deformation of the Indo-Australian Plate. *Journal of Geophysical Research: Solid Earth*, 96(B7), 11779–11802. https://doi.org/10.1029/91JB00897.

Sandwell D.T., Müller R.D., Smith W.H.F., Garcia E. & Francis R., 2014. New global marine gravity model from CryoSat-2 and Jason-1 reveals a buried tectonic structure. *Science*, 346, 6205, 65–67. https://doi.org/10.1126/science.1258213.

Sclater J.G. & Fisher R.L., 1974. Evolution of the East: Central Indian Ocean, with Emphasis on the Tectonic Setting of the Ninetyeast Ridge. *Geological Society of America Bulletin*, 85(5), 683–702. https://doi.org/10.1130/0016-7606(1974)85<683:EOTECI>2.0.CO;2.

Spector A. & Grant F.S., 1970. Statistical models for interpreting aeromagnetic data. *Geophysics*, 35(2), 293–302. https://doi.org/10.1190/1.1440092.

Sreejith K.M., Krishna K.S. & Bansal A.R., 2008. Structure and isostatic compensation of the Comorin Ridge, north central Indian Ocean. Geophysical Journal International, 175(2), 729–741. https://doi.org/10.1111/j.1365-246X.2008.03905.x.

Sreejith K.M., Radhakrishna M., Krishna K.S. & Majumdar T.J., 2011. Development of the negative gravity anomaly of the 85 E Ridge, north-eastern Indian Ocean – A process oriented modelling approach. *Journal of Earth System Science*, 120(4), 605–615. https://doi.org/10.1007/s12040-011-0099-9.

Sreejith K.M., Rajesh S., Majumdar T.J., Rao G.S., Radhakrishna M., Krishna K.S. & Rajawat A.S., 2013. High-resolution residual geoid and gravity anomaly data of the northern Indian Ocean – An input to geological understanding. *Journal of Asian Earth Sciences*, 62, 616–626. https://doi.org/10.1016/j.jseaes.2012.11.010.

Sreejith K.M., Unnikrishnan P. & Radhakrishna M., 2019. Isostasy and crustal structure of the Chagos–Laccadive Ridge, Western Indian Ocean: Geodynamic implications. *Journal of Earth System Science*, 128(6), 1–13. https://doi.org/10.1007/s12040-019-1161-2.

Stein S. & Okal E.A., 1978. Seismicity and tectonics of the Ninetyeast Ridge area: Evidence for internal deformation of the Indian plate. *Journal of Geophysical Research: Solid Earth*, 83(B5), 2233–2245. https://doi.org/10.1029/JB083iB05p02233.

Stein C.A., Cloetingh S. & Wortel R., 1989. Seasatderived gravity constraints on stress and deformation in the northeastern Indian Ocean. *Geophysical Research Letters*, 16(8), 823–826. https://doi.org/10.1029/GL016i008p00823.

Straume E.O., Gaina C., Medvedev S., Hochmuth K., Gohl K., Whittaker J.M., Abdul Fattah R. et al., 2019. GlobSed: Updated total sediment thickness in the world's oceans. *Geochemistry, Geophysics, Geosystems*, 20(4), 1756–1772. https://doi.org/10.1029/2018GC008115.

Subrahmanyam M. & Gebissa F.T., 2017. Performance evaluation of spectral analysis and Werner deconvolution interpretation techniques in magnetic method. *Journal of Applied Geophysics*, 138, 102–113. https://doi.org/10.1016/j.jappgeo.2017.01.017.

Subrahmanyam C. & Singh R.N., 1992. Geotectonics of the Bay of Bengal. *Indian Journal of Petroleum Geology*, 1, 161–180.

Werner S., 1953. *Interpretation of Magnetic Anomalies at Sheet-like Bodies*. Sveriges geologiska undersökning. Ser. C. Avhandlingar och uppsatser, 508, Norstedt, Stockholm.

Wessel P., Matthews K., Müller R., Mazzoni A., Whittaker J., Myhill R. & Chandler M., 2015. Semi-automatic fracture zone tracking. *Geochemistry, Geophysics, Geosystems*, 16(7), 2462–2472. https://doi.org/10.1002/2015GC005853.